JBMR Plus, 2025, **9**, ziaf038
https://doi.org/10.1093/jbmrpl/ziaf038
Advance access publication: March 2, 2025
Research Article

Alpha-smooth muscle actin-expressing dermal sheath cells are a major cellular contributor to heterotopic subcutaneous ossifications in a mouse model of Albright hereditary osteodystrophy

Patrick McMullan[1,2], Peter Maye[2], Sierra H. Root[2], Qingfen Yang[1,2], Sarah Edie[3], David Rowe[2], Ivo Kalajzic[2], Emily L. Germain-Lee[1,2,4,*]

[1]Department of Pediatrics, University of Connecticut School of Medicine, Farmington, CT 06030, United States
[2]Department of Reconstructive Sciences, Center for Regenerative Medicine and Skeletal Development, University of Connecticut School of Dental Medicine, Farmington, CT 06030, United States
[3]The Jackson Laboratory, Farmington, CT 06032, United States
[4]Division of Endocrinology & Diabetes, Albright Center, Connecticut Children's, Farmington, CT 06032, United States
*Corresponding author: Emily L. Germain-Lee, Pediatric Endocrinology, University of Connecticut School of Medicine and Connecticut Children's, 505 Farmington Ave, 2nd Floor, Farmington, CT 06032, United States (GermainLee@uchc.edu)

Abstract

Heterotopic ossifications (HOs) are the pathologic process by which bone inappropriately forms outside of the skeletal system. Despite HOs being a persistent clinical problem in the general population, there are no definitive strategies for their prevention and treatment due to a limited understanding of the cellular and molecular mechanisms contributing to lesion development. One disease in which the development of heterotopic subcutaneous ossifications (SCOs) leads to morbidity is Albright hereditary osteodystrophy (AHO). Albright hereditary osteodystrophy is caused by heterozygous inactivation of *GNAS*, the gene that encodes the α-stimulatory subunit ($G\alpha_s$) of G proteins. Previously, we had shown using our laboratory's AHO mouse model that SCOs develop around hair follicles. Here we show that SCO formation occurs due to inappropriate expansion and osteogenic differentiation of cells that express alpha-smooth muscle actin and that are located within the dermal sheath. We also show in AHO patients and mice that *secreted frizzled related protein 2* (*SFRP2)* expression is upregulated in regions of SCO formation and that elimination of *Sfrp2* in male AHO mice leads to earlier development, greater severity, and acceleration of formation of SCOs. These studies provide key insights into the cellular and molecular mechanisms contributing to SCO development and have implications for potential therapeutic modalities not only for AHO patients but also for patients suffering from HOs with other etiologies.

Keywords: Albright hereditary osteodystrophy, pseudohypoparathyroidism, pseudopseudohypoparathyroidism, *GNAS*, heterotopic ossification, subcutaneous ossification, dermal sheath, hair follicle, SFRP2, secreted frizzled related protein 2

Lay Summary

Albright hereditary osteodystrophy (AHO) is a condition caused by mutations in a gene called *GNAS*. It is frequently accompanied by bone deposits that form under the skin, termed subcutaneous ossifications (SCOs). Subcutaneous ossifications often lead to significant pain and decreased functional capabilities. We are interested in the mechanisms involved in SCO formation, and through use of our mouse model of AHO as well as what we learn from patients with this condition, our goal is to develop treatments not only for AHO but also for patients who develop deep ossifications such as those from hip fracture repairs, burns, and blast injuries.

Introduction

Heterotopic ossifications (HOs) are the result of a pathologic process by which bone inappropriately forms outside of the skeletal system in areas such as the dermis, subcutaneous tissue, and skeletal muscle[1,2] and are a significant clinical issue in the general population. Heterotopic ossifications frequently form after surgical procedures such as hip arthroplasty (up to 40%), as well as close to 30% of fractures, high-energy military injuries, severe burns, and up to 50% of traumatic brain and spinal cord injuries.[1] Although non-genetic forms of HOs are a major clinical issue, there are no definitive therapeutic strategies for their prevention and treatment. This lack of available therapies is problematic because HOs not only can cause pain and joint immobility but also can cause permanent neurologic damage and vascular insufficiency if inappropriately managed.[1,2] Furthermore, surgical resection of HOs is often not an option due to frequent postoperative recurrence.[1,2]

A definitive strategy for the prevention and treatment of HOs requires a better understanding of the cellular populations contributing to their formation and the molecular mechanisms promoting aberrant osteogenesis. One approach toward understanding these etiologies is to study monogenic disorders that result in spontaneous heterotopic bone formation. To date, there are 3 monogenic disorders that are characterized by the formation of extensive HOs. The most

Received: October 28, 2024. **Revised:** February 19, 2025. **Accepted:** February 26, 2025

devastating in terms of HO severity is fibrodysplasia ossificans progressiva (FOP), which has been shown to be caused by mutations in the gene encoding activin A receptor type 1 (*ACVR1*).[3] This mutation results in the hyperactive dysregulation of the BMP signaling cascade leading to endochondral bone formation within skeletal muscle and surrounding connective tissue.[3] Two additional disorders that result in spontaneous HO formation include Albright hereditary osteodystrophy (AHO) and progressive osseous heteroplasia (POH) (for review, see[4–7]).

Albright hereditary osteodystrophy is a disorder caused by the heterozygous inactivation of *GNAS*, an imprinted gene that encodes the α-stimulatory subunit (Gαs) of G protein-coupled receptors, which are utilized by multiple hormones that activate adenylyl cyclase (for review, see[4–7]). Patients with maternally inherited *GNAS* mutations develop pseudohypoparathyroidism type 1A (PHP1A) and exhibit extraskeletal manifestations that include obesity and resistance to multiple hormones requiring Gαs, such as PTH, TSH, GHRH, and LH/FSH, whereas patients with paternally derived *GNAS* mutations develop pseudopseudohypoparathyroidism (PPHP), in which patients have AHO skeletal features without severe obesity or hormonal resistance (for review, see[4–7]). Through studies of both humans and mouse models[4] these metabolic and hormonal distinctions were shown to be due to tissue-specific paternal imprinting of *GNAS*, typically within endocrine organs such as the pituitary, thyroid, gonads, renal cortex, and potentially osteoclasts (for review, see[4–7]).

Progressive osseous heteroplasia is also attributed to heterozygous inactivation of *GNAS*, secondary to paternal inheritance of the affected allele, and in general POH patients do not have hormonal resistance,[8,9] although there are rare cases of an overlap syndrome with PHP1A.[10,11] Unlike lesions in FOP, the HOs that form within AHO and POH develop within the skin and subcutaneous tissue by intramembranous ossification for which the cellular and molecular mechanisms remain undetermined.[5,6,9,12,13] Although AHO and POH share a similar genetic defect, they are recognized clinically as 2 distinct disorders aside from the difference in hormonal resistance. First, the extent of penetration of HOs differs between the 2 conditions. In patients with AHO, heterotopic bone formation is always restricted to the dermis and subcutaneous tissue and does not penetrate further.[7,13] Our group has confirmed this through physical examinations of our AHO patient population as well as through clinically indicated radiographs, CT scans, and MRIs,[13] and this is recapitulated in our mouse model.[12] Therefore, heterotopic bone lesions that form in AHO are defined as subcutaneous ossifications (SCOs). Patients with POH, however, develop significantly more invasive heterotopic bone when compared to AHO, and although ossifications in POH can be identified within the dermis and subcutaneous tissue, these lesions often penetrate into underlying tissue such as skeletal muscle, fascia, tendons, and deep connective tissue.[5,6,9,12,13] The second distinction in the heterotopic bone between AHO and POH is that in addition to heterotopic bone formation, AHO patients develop additional skeletal manifestations including shortened stature and brachydactyly, whereas these are typically absent in POH.[5,6,9,12,13]

In our Albright Center, a clinic dedicated to the care of patients with AHO, we have evaluated hundreds of mutation-confirmed patients from throughout the world. Many suffer from pain and decreased functional abilities secondary to SCOs, and in this regard, we have become interested in determining the mechanisms involved in SCO initiation and formation; an understanding of this pathophysiology could provide insights into therapeutic modalities for prevention and treatment. Over a 16-yr timespan of monitoring a cohort of 67 mutation–confirmed AHO patients, we found that SCOs are present at an equal prevalence of approximately 70% in both PHP1A and PPHP.[13] These lesions develop de novo as early as birth and/or secondary to repetitive pressure or trauma. Further observation of this patient cohort revealed that SCO prevalence was significantly higher among male patients than females, suggesting the potential for sex hormones contributing to SCO development. Additionally, patients with nonsense or frameshift *GNAS* mutations developed SCOs at a significantly higher frequency (>90%) than patients with missense mutations (29.2%), suggesting a genotype–phenotype correlation.[13]

In conjunction with clinically monitoring AHO patients, we had generated and characterized an AHO mouse model via the targeted disruption of exon 1 of *Gnas* that recapitulates the human disorder.[12,14] In particular, mice with heterozygous inactivation of *Gnas* (*Gnas E1+/−*) develop SCOs that are independent of the parental origin of the mutant allele.[12,14] *Gnas E1+/−* mice form SCOs both spontaneously and/or in response to repetitive pressure or trauma, such as at the base of the tail, footpads, and surrounding ear tags, and CT examination of *Gnas E1+/−* mice revealed that SCOs are limited to the dermis and subcutaneous tissue.[12] Similar to AHO patients, male *Gnas E1+/−* mice have SCOs at a significantly higher prevalence than female mice, with 100% of male mice developing SCOs by 36 wk of age. Histologic evaluation revealed that prior to the formation of radiographically etectable SCOs, male *Gnas E1+/−* mice at 12 wk exhibit hypercellularity and collagen deposition within the reticular dermis that specifically surrounds hair follicles (HFs).[12] These histologic changes appear to be essential for the future development of SCOs since both male and female *Gnas E1+/−* mice at later timepoints develop SCOs that consistently form directly adjacent to or surrounding HFs. The HF is known to contain epithelial- and mesenchymal-derived progenitor populations that maintain their proliferative abilities throughout all phases of life,[15] and this consistent spatial localization of SCOs near HFs suggested the possibility that this microenvironment and its progenitor populations may play a role in ossification development.

This investigation is the first to demonstrate that SCO formation is initiated by the inappropriate expansion and differentiation of mesenchymal-derived HF-resident alpha-smooth muscle actin (αSMA)-expressing dermal sheath cells into osteoblasts.

Materials and methods

Generation and maintenance of mice

All animal studies and protocols were carried out in accordance with the standards of the UConn Health Animal Care and Use Committee. Mice were fed a standard diet of mouse chow and water *ad libitum*. Mouse strains and their background are outlined in Table S1. The generation of *Gnas E1+/−* mice carrying a targeted disruption of exon 1 of *Gnas*[12,14] as well as the generation and characterization of *Osx-mCherry*[16] mice and *αSMACre^{ERT2};Ai9$^{fl/fl}$*[17] mice have

been previously described. *Sfrp2*$^{tm1.1Brle}$ mice (from here on termed *Sfrp2−/−* mice) were purchased from Jackson Labs. *Gnas E1+/−*, *Sfrp2−/−*, and *αSMACre*^{ERT2}*;Ai9*$^{fl/fl}$ mice were maintained on a pure 129SvEv background. *Osx-mCherry* mice were maintained on a CD1 background; therefore for *Gnas E1+/−;Osx-mCherry* mice used for in vivo studies, the mice were bred as F1 129xCD1 crosses and the *Osx-mCherry* littermates were used as controls. Mice were genotyped by PCR analysis using the primer sequences outlined in Table S2. For experiments utilizing *αSMACre*^{ERT2}*;Ai9*$^{fl/fl}$ mice, Cre activation was performed by intraperitoneal injection of tamoxifen in corn oil (75 μg/g body weight). Mice were administered 2 doses of tamoxifen spaced 48 hours apart.

Mouse histology

Following euthanasia, dorsal skin hair was removed using an electric trimmer and a depilatory cream (Nair, Church & Dwight, New York, NY). Dorsal skin samples, including the underlying adipose and muscle, were harvested and fixed in 10% NBF overnight at 4 °C, followed by 30% sucrose in PBS for 24 hours at 4 °C and subsequently embedded into optimal cutting temperature matrix. Tissue blocks were stored at −20 °C until use, and cryosections (10-15 μm) were collected using a cryostat tape-transfer system (Section-lab, Hiroshima, Japan) as previously described.[18,19] Samples were imaged using a Ziess Axioscan Z1 high speed automated image acquisition system (Cat#440640-9903-000) and a high resolution camera (AxioCam HRm).

Bone mineral label visualization

WT and *Gnas E1+/−* mice were administered intraperitoneal injections of calcein [10 mg/kg (Sigma C-0875)] or alizarin complexone [30 mg/kg (Sigma A-3882)] 2-7 d prior to sacrifice. Dorsal skin sections were stained with calcein blue (Sigma M1255) for 10 min to visualize total mineral content, as previously described.[18,19] For multiplex staining, skin sections were decalcified using a sodium acetate and sodium tartrate dibasic dihydrate solution in water (pH 4.2) to remove bone mineral labels from the tissue section.

Immunofluorescence

Antibodies utilized for immunofluorescence staining are listed in Table S3. Tissues were permeabilized in 0.1% Triton X for 10 min, blocked using a Mouse-on-Mouse Immunodetection Kit (Vector Laboratories BMK-2202) diluted in a 2% bovine serum albumin in PBS solution for 45 min, and stained with primary antibody overnight at 4 °C. The following day, sections were washed in 0.1% Triton X in PBS for 10 min and stained with secondary antibodies (1:300 dilution) in 2% BSA in PBS at room temperature for 1 hour. Tissue sections were mounted in a 50% glycerol / PBS solution containing 4',6-diamidino-2-phenylindole (DAPI) (1:1000 dilution) and imaged.

Alkaline phosphatase enzyme histochemistry

Alkaline phosphatase (ALP) enzyme histochemistry was performed on tissue sections following the methods previously described.[18,19] Briefly, slides were incubated in an alkaline buffer (1 M Tris, 1 M $MgCl_2$, 2 M NaCl in deionized water pH 9.5) for 10 min, followed by exposure to an alkaline Fast Red substrate buffer for 30 min. Sections were mounted in 50% glycerol/PBS solution with DAPI and coverslipped for image acquisition. For experiments performed with *Osx-mCherry* and *αSMA-CRE*^{ERT2}*;Ai9*$^{fl/fl}$ reporter mice, ALP staining was performed using a Vector Blue Alkaline Phosphatase Substrate Kit (Vector Laboratories SK-5300) for 30 min to avoid overlap of fluorescent signals.

Chromogenic staining

General tissue architecture within the dermis was visualized by staining tissues with 0.025% Toluidine blue in deionized water for 5 min as previously described.[18,19] Von Kossa staining was performed by incubating slides with a 4% silver nitrate solution and exposing slides to 2400 kJ of ultraviolet light using a UV Stratalinker. Safranin O and fast green staining was performed by staining sections in Weigert's Iron Hematoxylin for 5 min to visualize nuclei, rinsed in tap water for 10 min, stained in 0.2% fast green solution for 2 min, rinsed in 1% acetic acid solution for 2 min, and stained in 0.1% safranin O solution for 1 min. Masson Trichrome Staining was performed using a commercially available kit (Sigma HT15-1KT) based on the manufacturer's instructions.

Dorsal skin flow cytometry

Flow cytometry analyses were performed using single cell suspensions isolated by enzymatic digestion from 40 wk old *WT* and *Gnas E1+/−* dorsal skin samples using slightly modified methods as described by Walmsley et al. (2016).[20] Briefly, the entire dorsal skin was harvested, avoiding collection of underlying adipose or skeletal muscle, and placed in sterile PBS on ice. Harvested samples were minced into 1-2 mm fragments and placed into DMEM supplemented with 2 mg/mL Collagenase IV and 0.5 mg/mL Collagenase I. Collection beakers were then placed onto a magnetic stirrer at medium speed inside a cell culture incubator at 37 °C to promote tissue digestion. After 90 min of digestion, an equal amount of DMEM containing 10% FBS was added to the digested tissue sample, passed through a 100 μm filter and centrifuged at 300 g for 10 min at 4 °C. The collected cell pellet was resuspended in Zombie Fixable Live/Dead Staining Solution in PBS and incubated for 30 min at 4 °C protected from light. Samples were subsequently washed and centrifuged in Staining Media [Hanks' balanced salt solution (HBSS) supplemented with 10% FBS and 10 μg/mL DNase I]. The remaining pellet was stained for 20 min at 4 °C in Staining Media with primary conjugated antibodies for cell surface markers (antibodies, clones, and dilution factors are summarized in Table S4). Stained cells were washed, centrifuged, fixed in 4% PFA for 15 min at 4 °C, and incubated in 1X InVitrogen eBioscience Cell Permeabilization buffer (InVitrogen 00-8333-56) for 15 min at 4 °C. After centrifugation, the resuspended pellet was stained with an Alexa-488 conjugated αSMA antibody clone 1A4 (1:100 dilution) for 30 min at 4 °C. Washed and filtered cells were analyzed with a BD-LSRII flow cytometer with gates established according to unstained and single-channel controls. All compensations were identified using FACS Diva Software, and downstream data analysis was performed using FlowJo Software v10.

Primary dermal explant cultures

Primary dermal explant cultures were established from dorsal skin fragments isolated from 40 wk *Gnas E1+/−;αSMA-CRE*^{ERT2}*;Ai9*$^{fl/fl}$ and *αSMA-CRE*^{ERT2}*;Ai9*$^{fl/fl}$ mice following methods as previously described by Seluanov et al. (2010).[21]

Confluent primary cell cultures were dissociated using Accutase, and subsequently prepared for either FACS or passaged onto 24-well culture dishes at a cellular density of 5.0×10^4 cells per well for osteogenic differentiation or collagen deposition assays. For experiments using recombinant Sfrp2 treatment, cultures were exposed for the duration of treatment with either 100 ng/mL recombinant mouse Sfrp2 (R&D Systems Cat 1169-FR-025) or vehicle control (PBS with 0.1% BSA).

Dermal explant FACS sorting

FACS analysis and cell sorting of Ai9+ cells from primary dermal explants were performed using a BD FACSAria II (BD Biosciences, San Jose, CA, United States). Primary cell culture pellets were resuspended into FACS Staining Media (HBSS supplemented with 10% FBS) containing Sytox Blue Dead Cell Stain (InVitrogen S34857). Sorting gates were established using cultures generated from non-transgenic cultures and unstained transgenic cultures. All downstream data analysis was performed using FlowJo in order to determine the percentage of Ai9+ sorted populations.

In vitro osteogenic differentiation assays

Osteogenic differentiation capacity was assessed in vitro by exposing cultures to DMEM/F12 with 10% FBS, 1% penicillin/streptomycin supplemented with 50 μg/mL ascorbic acid and 10 mM Beta-glycerophosphate for 28 d. Live imaging studies assessing bone mineralization was performed by supplementing culture media with 30 μM calcein (Sigma C-0875) overnight. The following day, areas of mineralization and their localization to Ai9+ populations were assessed by fluorescence microscopy. Cultures were subsequently fixed in 4% PFA and stained for ALP using the Vector Blue Alkaline Phosphatase Substrate Kit (Vector Laboratories SK-5300) and Von Kossa using a 4% silver nitrate solution and exposing cultures to 2400 kJ of ultraviolet light using a UV Stratalinker.

In vitro collagen deposition assays

Total collagen deposition from dermal explants cultured in DMEM/F12 containing 10% FBS for 14 d was assessed using a Sirius red/fast green assay as previously described.[22] Briefly, cells were fixed using a Kahle fixative solution and stained for 30 min in a 0.1% Fast Green and 0.2% Sirius Red solution in saturated picric acid in distilled water. Stained cultures were visualized under brightfield microscopy to assess collagen deposition and destained using a 0.1 N sodium hydroxide solution in absolute methanol for absorbance measurements at 540 and 605 nm. Calculations of total collagen per well using these absorbance measurements were performed based on the previously described methods.[22]

RNA purification

Total RNA was extracted from dermal explant cultures, FACS-sorted cultures, and 1 cm^2 dorsal skin samples using an RNEasy Micro Kit (Qiagen) for FACS-sorted cultures and a Direct-zol RNA Miniprep Kit (Zymo Research) for dermal explant and dorsal skin samples following the manufacturer's instructions. Prior to RNA isolation, harvested dorsal skin tissue was placed into RNA Later solution (InVitrogen) and stored at −80 °C. The tissue was thawed into RNA Later solution, minced into 1-2 mm fragments, and subsequently placed into 1 mL of Trizol (Invitrogen) on ice and homogenized. RNA samples were treated with DNAse I (New England Biosciences) and were concentrated through a Monarch RNA Cleanup Kit (NEB) to ensure no carryover of contaminants.

Quantitative RT-PCR

1 μg of RNA was utilized for reverse transcription using a high capacity cDNA reverse transcription kit (Applied Biosystems). Quantitative RT-PCR was performed using a Bio-Rad CFX96 ThermoCycler (Bio-Rad Laboratories, Hercules, CA) within a 20 μL reaction, consisting of iTaq Universal SYBR Green supermix (Bio-Rad Laboratories, Hercules, CA), 10 μM of forward and reverse primers, and 25 ng of cDNA. The specific primer sequences utilized are listed in Table S4.

Human *GNAS* mutation analyses of participants

All human studies were approved by the Johns Hopkins Medicine Institutional Review Board (E.L.G.-L.'s institution at that time). Informed consent was obtained from all participants (or parents of participants) prior to enrollment. Assent was obtained when appropriate based on age and emotional/cognitive maturity. In brief, peripheral blood from all participants was collected within the Johns Hopkins Institute of Clinical and Translational Research. DNA isolation and *GNAS* mutation analyses of the 13 coding exons and all intron/exon boundaries, including determination of the parental origin of the mutated allele, were performed for all participants in our investigations (E.L.G.-L., Johns Hopkins laboratory) as previously described.[23,24] Therefore, all participants were mutation-confirmed. We also documented that the POH participant in our study had inheritance of the mutation from the paternal allele, which is the pattern of inheritance typical of POH.[25] The participant with POH had very severe SCOs as well as deep, penetrating ossifications assessed by surgical pathology of excised ossifications as well as CT and MRI performed for clinical reasons.

Human dermal biopsy culture generation from mutation-confirmed AHO and POH participants

Informed consent and assent specifically for the skin biopsies were additionally obtained from all participants (or parents of participants) prior to enrollment. For consistency, skin biopsies were performed by the same investigator (E.L.G.-L.) on all participants with mutation-confirmed AHO (both PHP1A and PPHP) and POH, as well as on unaffected family members (in whom no *GNAS* mutations were identified). Skin biopsies were performed according to standard clinical procedures using a 2 mm biopsy punch (Accu-Punch Biopsy Punch, Accuderm Inc., Ft Lauderdale, FLA) after numbing the region with 1% lidocaine. Biopsies of SCO regions were performed on an extremity within a location of significant subcutaneous tissue. If no SCOs were present, biopsies were collected on the ventral surface of the participant's forearm. Primary cultures were generated and maintained in Minimum Essential Medium (Eagle's) with Earle's Salts supplemented with 85 units of penicillin and streptomycin/mL, 1.7 moles L-glutamine, and 13% FBS. RNA was extracted using a cesium chloride gradient. There were no complications post-procedure.

Microarray analyses from RNA generated from human dermal cultures

Microarray analyses were performed using RNA obtained from dermal fibroblast cultures from 5 mutation-confirmed participants, consisting of 4 with AHO and 1 with POH.

Participants with AHO with varying degrees of SCOs were chosen. The severity of SCOs was based on the number of individual lesions noted on palpation by one consistent examiner (E.L.G.-L.) and categorized as either none, minimal, moderate, or severe, with minimal < 3, moderate = 3-25, and severe > 25. The number of SCOs > 1.0 cm increased with the degree of severity.

All microarray analyses were performed by the Johns Hopkins Medical Institutions Microarray Core Facility using an Affymetric GeneChips U133 Plus 2.0 (human) chip (Santa Clara, CA). Differential gene expression was determined on the basis of exhibiting either > +2.0 fold or <−2.0 fold change as well as a having a probability of >0.50. Pairwise comparisons of these samples (ie, 2 participants analyzed and compared to one another) were performed. In all 3 comparisons (P1 × P2, P3 × P2, and P4 × P5), a participant with the greater number (and size as well) of SCOs was compared to a participant with fewer or no ossifications.

Human *SFRP2* northern blot studies

RNA isolation and Northern blot analysis from human cultured fibroblasts were performed as previously described[26] using 10 micrograms of RNA per lane and analyzed by phosphorimager quantitation (Bio-Rad, Hercules, CA) of the resulting autoradiograph of the Northern blot and expressed as a ratio of *SFRP2* to *S26*.[26] For these studies, there were an additional 2 participants with mutation-confirmed AHO, and therefore a total of 9 participants: 6 with AHO (2 with PHP1A and 4 with PPHP), 1 with POH, and 2 unaffected family members for whom sequencing revealed no mutation in *GNAS*.

Statistical analysis

All statistical analyses were performed using Graphpad Prism Version 9 (GraphPad Software, Inc., La Jolla, CA, United States) with p-values <.05 considered statistically significant. For all analyses that compared data obtained from *WT* and *Gnas E1+/−* mice at one discrete time point (ie, Flow and FACS analyses and cell culture RT-PCR studies), data were analyzed using an unpaired 2-tailed t-test. For all analyses observed at one discrete timepoint comparing data from 3 or more groups, the data were analyzed by a one-way ANOVA with a post hoc Tukey test for multiple comparisons. p-values for each statistical comparison are indicated within the figure panels.

Results

Gnas E1+/− mice develop SCOs that progressively expand and localize to HFs

We utilized an AHO mouse model generated within our laboratory to investigate the cellular and molecular mechanisms contributing to SCO formation.[14] This model was generated through the targeted disruption of exon 1 of the gene *Gnas*, which leads to the global heterozygous inactivation of *Gnas (Gnas E1+/−)*.[14] Serial X-rays of *Gnas E1+/−* mice demonstrated that SCOs become radiographically detectable by 16 wk of age and progressively expand (Figure 1A). Histologic analysis of 40 wk *Gnas E1+/−* dorsal skin samples demonstrates that SCO formation occurs through intramembranous ossification as indicated by enhanced collagen and osteoid deposition along the bone lining surface by Masson Trichrome staining and the absence of glycosaminoglycan detection by Safranin O staining (Figure S1A and B). We also found that this progressive expansion of intramembranous heterotopic bone surrounding HFs in *Gnas E1+/−* mice is the result of bone remodeling as reflected by the presence of actively mineralizing osteoblasts (Figure 1B) and bone-lining osteoclasts (Figure S1C).

To assess the potential presence and spatial localization of HF-resident cell types contributing to SCOs within *WT* and *Gnas E1+/−* mice, we performed ALP enzyme histochemistry in dorsal skin sections of 80 wk old mice (Figure 1C-F). Both *WT* (Figure 1C) and *Gnas E1+/−* (Figure 1D) mice displayed ALP+ populations within the HF that localized to a distinct mesenchymal population, specifically the dermal papilla. However, *Gnas E1+/−* mice in SCO-containing regions exhibit an expansion of ALP+ cells within 2 additional areas of the dermis including: (1) the SCO bone-lining surface; and (2) the adjacent unmineralized regions of the dermis encompassing the entire HF (Figure 1D-F). These data align with previous studies in our laboratory demonstrating *Gnas E1+/−* mice develop SCOs within the HF microenvironment[12] and that the formation of these lesions may be driven by the expansion of an HF-resident cell population.

Osterix-mCherry reporter identifies expanded αSMA+ dermal sheath cell population in vivo leading to intramembranous ossification within *Gnas E1+/−* mice

To further characterize the presence and spatial localization of HF-resident cells giving rise to the SCOs, we crossed *Gnas E1+/−* mice with an *Osterix-mCherry* (*Osx-mCherry*) transgenic reporter model to label osteoprecursors, osteoblasts, and osteocytes in vivo (Figure S2A).[16] We were particularly interested in utilizing this model to examine *Gnas E1+/−* skin regions prior to the formation of radiographically detectable SCOs given our previous studies demonstrating the presence of hypercellularity and collagen deposition near HFs, which we hypothesize represents condensation of an HF-resident cell population initiating intramembranous ossification.[12]

We identified a distinct population of Osterix+ cells within both *Gnas E1+/−;Osx-mCherry* and *Osx-mCherry* littermate controls that localized to the outer surface of the HF at 3 wk (Figure S2B and C), 24 wk (Figure 2A-E), and 40 wk (Figure S2D,E). We detected a markedly significant expansion of dermal Osterix+ cell populations within *Gnas E1+/−;Osx-mCherry* mice at 24 wk (Figure 2C-E) when compared to littermate *Osx-mCherry* controls within skin regions without radiographically detectable SCOs. We also demonstrate using ALP enzyme histochemistry that these expanded Osterix+ cells in *Gnas E1+/−;Osx-mCherry* mice coexpressed ALP (Figure 2E) and may represent the same ALP+ cells in the HF environment that we previously identified.

Further immunofluorescence colocalization revealed these Osterix+ HF-resident populations in *Gnas E1+/−;Osx-mCherry* and *Osx-mCherry* mice corresponded to dermal sheath cells based upon their co-expression of αSMA, which is an established biomarker for this cell type (Figure 2D).[27] These data demonstrating Osterix and αSMA colocalization were of particular interest, because in addition to being an established marker for dermal sheath cells, αSMA has

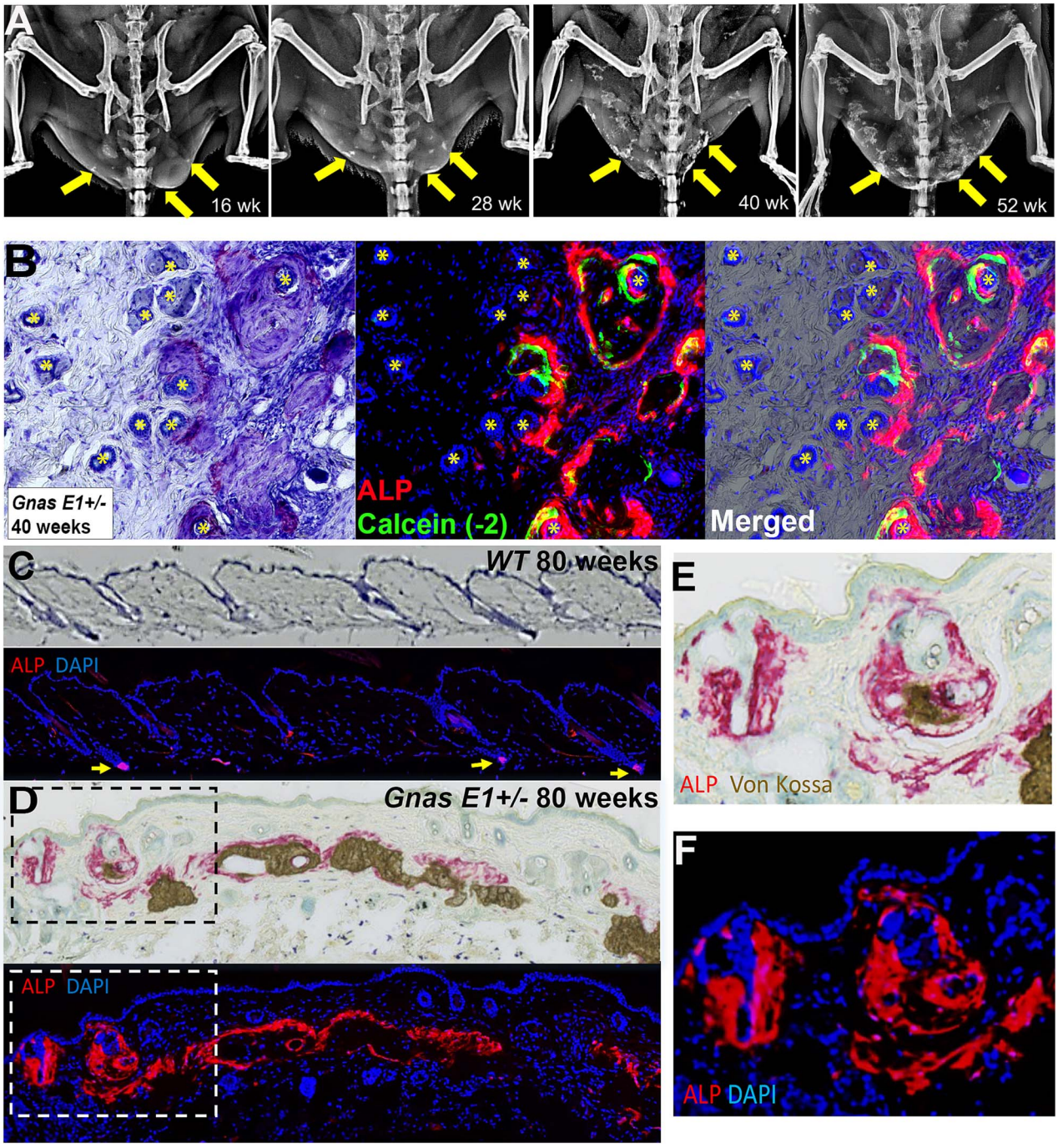

Figure 1. *Gnas E1+/–* mice develop progressively expanding subcutaneous ossifications in dermis surrounding hair follicles. (A) Consecutive X-ray images of a male *Gnas E1+/–* mouse at 16, 28, 40, and 52 wk. (B) Dorsal skin of 40-wk-old male *Gnas E1+/–* mouse stained with toluidine blue and ALP to demonstrate SCOs surrounding hair follicles and the presence of active mineralizing osteoblasts [alkaline phosphatase (ALP+) populations superimposed over a calcein mineralization label]. (C-D) Dorsal skin sections from 80 wk old (C) *WT* and (D) *Gnas E1+/–* mice stained using toluidine blue, ALP, and Von Kossa. ALP+ populations within *WT* mice are limited to the dermal papilla (arrows) whereas *Gnas E1+/–* mice display ALP+ cells within the dermal papilla and throughout the dermis along the SCO bone surface. (E-F). Higher power images of boxed regions in panel (D). Abbreviations: ALP, alkaline phosphatase; SCO, subcutaneous ossification.

been previously identified as a biomarker for tissue-resident mesenchymal progenitors with osteogenic potential that contribute to HO formation within skeletal muscle.[17,28,29] We further demonstrate in Figure 2E that the expanded Osterix and ALP double positive cells within the dermis of *Gnas E1+/–;Osx-mCherry* mice were additionally αSMA+. Collectively, these data aligned with our initial hypothesis and suggest that these Osterix+, αSMA+, ALP+ triple positive cells within the dermis are labeling expanded dermal sheath cells actively undergoing osteogenic differentiation.

We next further examined the contribution of dermal-resident αSMA+ populations to SCO formation within 40 wk old mice, as *Gnas E1+/–* mice at this timepoint consistently exhibit SCOs throughout the dorsal skin

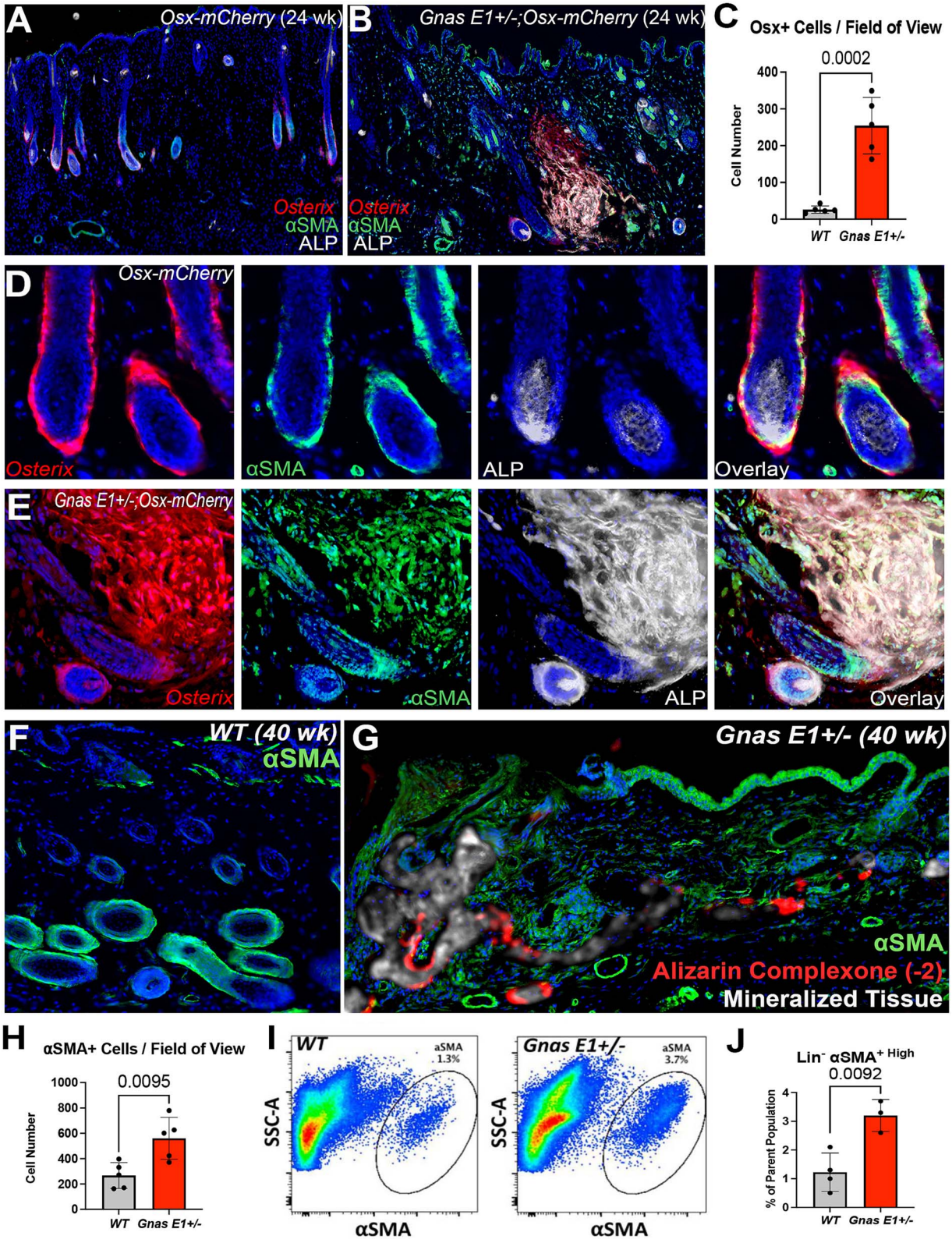

Figure 2. *Osterix-mCherry* transgenic reporter model identifies αSMA+ dermal sheath cells. (A-B) Dorsal skin sections of 24 wk (A) *Osx-mCherry* and (B) *Gnas E1+/−;Osx-mCherry* littermates demonstrating spatial expression of *Osterix* (red), αSMA (green), and ALP (white). (C) Bar graph demonstrating number of *Osterix*+ cells within the dermis of 24 wk *Osx-mCherry* and *Gnas E1+/−;Osx-mCherry* mice. (D-E) Higher-power images of (D) *Osx-mCherry* and (E) *Gnas E1+/−;Osx-mCherry* hair follicles demonstrating *Osterix,* ALP, and αSMA colocalization. (F-G) Representative dorsal skin sections of 40 wk (F) *WT* and (G) *Gnas E1+/−* mice stained for αSMA (green), mineralized tissue (white), and bone mineral label alizarin complexone (red). (H) Bar graph demonstrating number of αSMA+ cells within the dermis of 40 wk *WT* and *Gnas E1+/−* mice. (I) Representative flow cytometry plots. SSC-A refers to side scatter area. (J) Graph of the percentage of Lin- αSMA+ populations from 40 wk *WT* and *Gnas E1+/−* mice in vivo. Abbreviations: αSMA, alpha-smooth muscle actin; ALP, alkaline phosphatase.

(Figure 2F-J). Alpha-SMA immunofluorescence within unaffected *WT* and *Gnas E1+/−* dorsal skin regions labeled HF dermal sheath cells, HF arrector pili muscles, and underlying vasculature, as similarly observed at earlier timepoints (Figure 2F). However, *Gnas E1+/−* mice exhibited a significant expansion of αSMA+ populations overlaying areas of active bone mineralization, as indicated by alizarin complexone labeling (Figure 2G and H), in addition to the surrounding dermis and the dermal-epidermal junction. We found a similarly diffuse distribution pattern when examining the dorsal skin of 40 wk old *Gnas E1+/−;Osx-mCherry* mice overlaying SCO sites (Figure S2E), and we therefore hypothesized this diffuse distribution may also be indicative of reactive myofibroblasts and pericytes in response to SCO lesion development. In addition to histologic analysis, flow cytometry on single cell suspensions of enzymatically digested dorsal skin samples from 40 wk *WT* and *Gnas E1+/−* mice revealed a 3-fold increase in the total percentage of αSMA+ mesenchymal progentiors within the Lineage-gate, which excluded hematopoietic and endothelial cells by CD45-Ter119- and CD31- staining, when compared to *WT* samples (Figure 2I and J, Figure S3A). In summary, these data suggest that αSMA+ cell populations may function as a contributing cell type during SCO development.

Lineage tracing utilizing *Gnas E1+/−;αSMA^{CreERT2};Ai9$^{fl/fl}$* model system identifies αSMA+ dermal sheath cell population capable of osteogenic differentiation into osteoblasts and osteocytes within SCOs

In order to demonstrate more definitively that αSMA+ dermal sheath cells are an indispensable population for the initiation of SCO formation, we performed genetic fate-mapping studies by crossing our *Gnas E1+/−* mouse model with a tamoxifen-inducible *αSMACre^{ERT2};Ai9$^{fl/fl}$* mouse model (Figure 3A).[17] This model system allowed us to trace αSMA+ cell types within the skin of both *Gnas E1+/−;αSMACre^{ERT2};Ai9$^{fl/fl}$* mice and littermate *αSMACre^{ERT2};Ai9$^{fl/fl}$* controls following the injection of tamoxifen through the expression of Ai9 (tdTomato). We first injected 8 wk old *Gnas E1+/−;αSMACre^{ERT2};Ai9$^{fl/fl}$* mice and littermate *αSMACre^{ERT2};Ai9$^{fl/fl}$* controls and performed a 24 wk lineage trace following tamoxifen injection (Figure 3B-H, Figure S3B). In alignment with previous αSMA lineage tracing studies in the skin,[27] we observed that 2 d following tamoxifen administration, Ai9 expression within 8 wk old *Gnas E1+/−;αSMACre^{ERT2};Ai9$^{fl/fl}$* mice and littermate *αSMACre^{ERT2};Ai9$^{fl/fl}$* controls were localized to the dermal sheath, HF arrector pili muscle, and underlying blood vasculature. Histologic evaluation in *αSMACre^{ERT2};Ai9$^{fl/fl}$* mice demonstrated that Ai9+ populations following a 24 wk lineage trace remained restricted to the dermal sheath, arrector pili, and blood vasculature (Figure 3C). Conversely, within the surrounding HF microenvironment, *Gnas E1+/−;αSMACre^{ERT2};Ai9$^{fl/fl}$* mice displayed a robust expansion of Ai9+ and ALP+ populations (Figure 3D-G), with colocalization studies revealing that these expanded Ai9+ populations coexpressed ALP (Figure 3E and G), localized to the SCO bone-lining surface superimposed over a calcein mineral label, and were embedded within the SCO bone matrix. Additionally, colocalization studies revealed 69% of the expanded dermal ALP+ populations within *Gnas E1+/−;αSMACre^{ERT2};Ai9$^{fl/fl}$* mice coexpressed Ai9 (Figure 3H). Taken together, these data demonstrate HF-resident αSMA+ dermal sheath cells are capable of undergoing differentiation into both osteoblasts and osteocytes and are the predominant essential cell type required for initial osteoid deposition and formation of SCOs.

In conjunction with in vivo lineage tracing, we assessed the osteogenic capacity of labeled Ai9+ populations in vitro by injecting 36 wk old *Gnas E1+/−;αSMACre^{ERT2};Ai9$^{fl/fl}$* and *αSMACre^{ERT2};Ai9$^{fl/fl}$* mice with tamoxifen at 7 and 5 d prior to tissue harvest and then generating primary dermal explant cell cultures (Methods described[21]) (Figure 3I). This culture model allowed us to monitor the behavior of Ai9+ cells from the onset of culture establishment and throughout the course of our in vitro analyses (Figure 3J) using live cell imaging. Following 14 d of primary culture expansion, we performed FACS sorting analyses and confirmed a 3-fold increase in the percentage of Ai9+ populations in *Gnas E1+/−;αSMACre^{ERT2};Ai9$^{fl/fl}$* cultures compared to *WT αSMACre^{ERT2};Ai9$^{fl/fl}$* (Figure 3K and L, Figure S3B). Gene expression studies demonstrated that Ai9+ sorted populations from *Gnas E1+/−* cultures have significant upregulation of *Osterix* (*Sp7*) mRNA expression when compared to *WT* Ai9+ and both *Gnas E1+/−* and *WT* unsorted cultures (Figure 3M). Additionally, *Gnas E1+/−* cultures following 28 d in osteogenic induction media displayed multiple colonies of ALP+ populations and mineral deposition by Von Kossa staining (Figure 3J), and live cell imaging demonstrated the in vivo labeled Ai9+ populations localized to areas of active mineralization based upon calcein staining (Figure 3J). This enhanced mineralization capacity in *Gnas E1+/−;αSMACre^{ERT2};Ai9$^{fl/fl}$* cultures correlated with an upregulation in both *Osterix (Sp7)* and *Integrin Binding Sialoprotein* (*Ibsp*) mRNA expression by RT-PCR when compared to *αSMACre^{ERT2};Ai9$^{fl/fl}$* cultures (Figure 3N). These data further implicate dermal αSMA+ progenitors as an essential cell type in SCO formation.

Gnas E1+/− mice exhibit transcriptome variation within SCO containing regions

We next investigated potential signaling pathways that may be promoting the inappropriate differentiation of these dermal populations by isolating RNA from dorsal skin samples from 52 wk *WT* mice and *Gnas E1+/−* mice from both unaffected and SCO-containing skin regions and assessing transcriptional variations among samples using an RT-PCR array (Figures S4 and S5). We were particularly focused on a panel of genes related to Wnt, Sonic hedgehog (Shh), TGF-β, and BMP signaling pathways due to their implications in regulating both epithelial-mesenchymal interactions within the HF microenvironment[30] and the pathogenesis of HOs. We did not identify any significant differences in mRNA expression patterns between *WT* and unaffected *Gnas E1+/−* skin samples, but we observed significant transcriptional changes in genes related to each of these canonical signaling pathways within SCO-containing *Gnas E1+/−* skin samples when compared to both *WT* and unaffected *Gnas E1+/−* samples (Figures S4 and S5). We also confirmed the validity of these transcriptomic data by performing immunofluorescence within dorsal skin specimens from 52 wk *WT* and *Gnas E1+/−* mice (Figure S4B-E), which demonstrated increased Gli1+ cellular populations (Figure S4B and C) in addition to

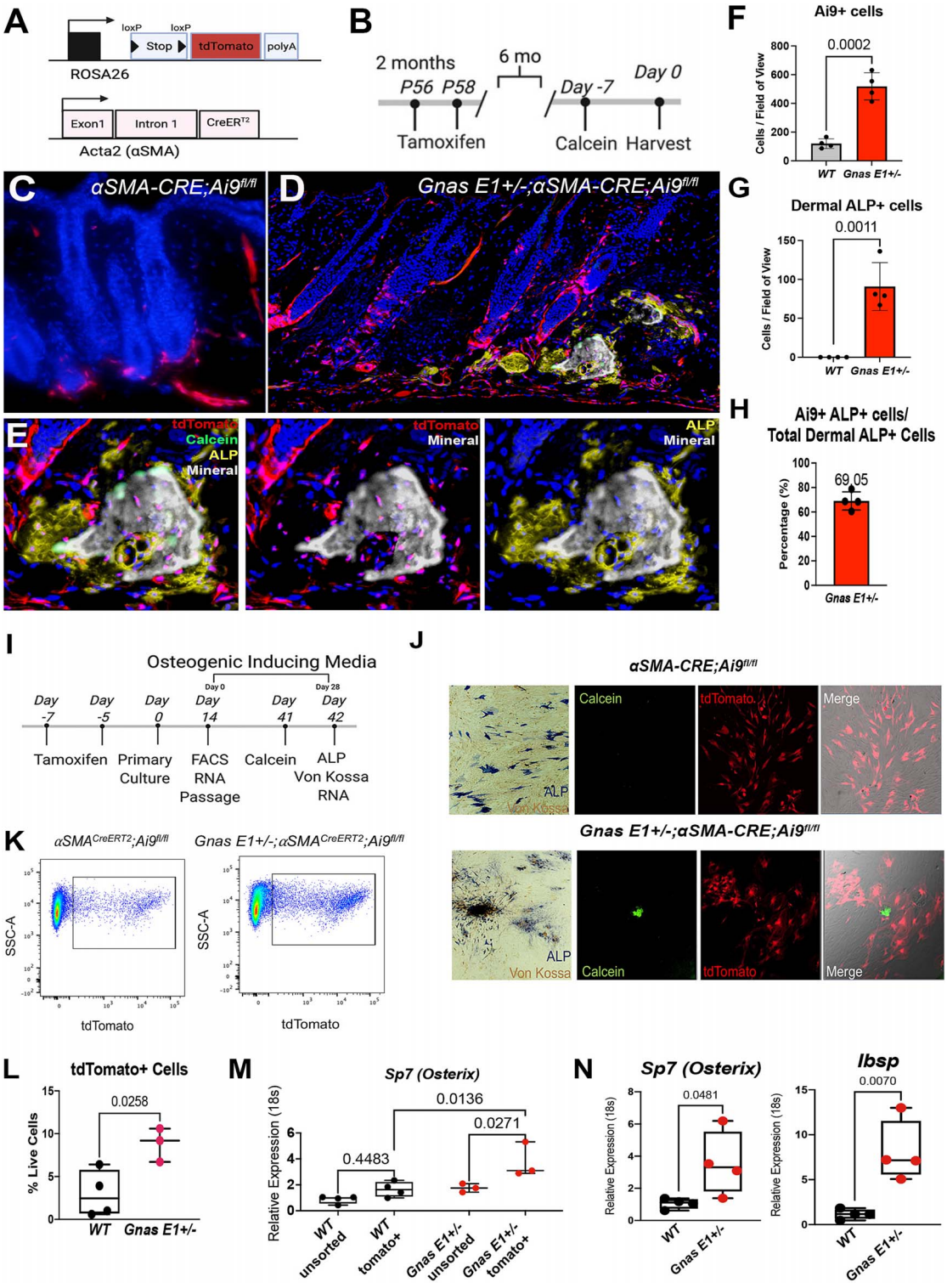

Figure 3. Lineage tracing of αSMA+ populations identifies hair follicle dermal sheath cells as contributing to SCO formation. (A) Breeding scheme and generation of *Gnas E1+/−;αSMACre^{ERT2};Ai9$^{fl/fl}$* mice. (B) In vivo lineage tracing strategy utilized. (C-E) Dorsal skin sections of 32 wk old mice: (C) *αSMACre^{ERT2};Ai9$^{fl/fl}$* and (D) *Gnas E1+/−;αSMACre^{ERT2};Ai9$^{fl/fl}$* following 6-mo lineage tracing study of Ai9+ populations also shown at higher magnification in (E) in which *Gnas E1+/−;αSMACre^{ERT2};Ai9$^{fl/fl}$* mice displayed an expansion of Ai9+ populations near hair follicles and differentiated into SCO-lining osteoblasts (ALP+ cells over calcein label) and osteocytes embedded into SCO bone matrix. (F) Bar graph demonstrating number of Ai9+ cells within dermis of *αSMACre^{ERT2};Ai9$^{fl/fl}$* and *Gnas E1+/−;αSMACre^{ERT2};Ai9$^{fl/fl}$* following 6-mo lineage tracing. (G,H) Graph of (G) number of dermal ALP+ cells and (H) percentage of dermal Ai9+;ALP+ double positive cells when compared to the total number of dermal ALP+ cells within 32 wk *Gnas E1+/−;αSMACre^{ERT2};Ai9$^{fl/fl}$* mice. (I) Timeline of dermal explant culture generation and in vitro lineage tracing. (J) Representative images *αSMACre^{ERT2};Ai9$^{fl/fl}$* and *Gnas E1+/−;αSMACre^{ERT2};Ai9$^{fl/fl}$* dermal explant cultures following 28 d of osteogenic differentiation stained for ALP and Von Kossa as well as live culture images of calcein (green) and tdTomato (red). (K) FACS plots and (L) graph of the percentage of Ai9+ cells isolated from *αSMACre^{ERT2};Ai9$^{fl/fl}$* and *Gnas E1+/−;αSMACre^{ERT2};Ai9$^{fl/fl}$* cultures. (M) RT-PCR of *Sp7* (*Osterix*) mRNA expression for unsorted and Ai9+ sorted primary dermal explants. (N) RT-PCR of *Sp7* and *Ibsp* mRNA expression in cultures following 28 d of osteogenic differentiation. Abbreviations: αSMA, alpha-smooth muscle actin; ALP, alkaline phosphatase; SCO, subcutaneous ossification.

Tgfβ1+ populations (Figure S4D and E) throughout the basal epithelium, dermis, and SCO bone-lining surface of *Gnas E1+/−* skin samples when compared to *WT*. In summary, these findings suggest that *Gnas* heterozygous inactivation results in the dysregulation of multiple signaling pathways within the HF microenvironment to promote the osteogenic differentiating capacity of tissue-resident cell populations that lead to SCO formation.

Identification of differentially-expressed genes associated with SCO formation in human fibroblasts isolated from AHO and POH participant skin biopsies

As an additional investigation to identify genes and/or pathways that may play a role in SCO formation, we performed a microarray analysis on RNA from primary dermal fibroblast cultures generated from skin biopsies from a selected group of mutation-confirmed AHO and POH participants. The participants selected either lacked SCOs or had SCOs of varying severity: Participant 1 (P1) was an adult female with PPHP with moderate palpable SCOs; Participant 2 (P2) was an adult female with PPHP without palpable SCOs; Participant 3 (P3) was a female child, daughter of P2, with PHP1A and severe SCOs; Participant 4 (P4) was an adult male with POH and extensive ossifications in the subcutaneous and deep connective tissue that invaded into the muscle, nerve, and blood vessels as documented by both surgical pathology of excised ossifications and imaging performed for clinical reasons (CT and MRI). Participant 5 (P5) was an adolescent male with PPHP and one small palpable SCO. We selected this diverse subgroup for analysis to examine both pre- and post-pubertal males and females with PHP1A and PPHP, and differences between close relatives differing in the extent of SCO formation.

We compared differential gene expression by performing 3 comparisons (Figure 4A) that we hypothesized would have the greatest potential of highlighting variations in expression based on the degree of SCO formation and that would also help sort out potential hormonal effects that could be leading to SCOs being worse in males than in females based on our past studies in both humans and our mouse model.[12,13] In all 3 comparisons (P1 vs P2, P3 vs P2, and P4 vs P5), a participant with the greater number (and size as well) of SCOs was compared to a participant with fewer or no ossifications. We identified 23 differentially regulated genes (14 upregulated and 9 downregulated) that were observed within SCO-containing regions in each comparison (Figure 4B and C). The 2 most upregulated genes were Rho GTPase activating protein 28 (*ARHGAP28*) and secreted frizzled related protein 2 (*SFRP2*), which have been shown to become activated in response to extracellular matrix assembly and negatively regulate stress fiber formation both in vivo and in vitro.[31–33] Prior reports have shown *SFRP2* functions as a secreted protein that binds and inhibits ligands essential for Wnt and BMP signaling.[33,34] Furthermore, it has been shown using a myocardial infarction injury model that administration of recombinant SFRP2 can limit type I collagen synthesis and ectopic mineralization by cardiac fibroblasts and mesenchymal progenitors in vivo.[33,34] Microarray analysis also demonstrated an upregulation in *ALDH1A3* and *NR4A3*, which are genes that have since been identified as being commonly recognized biomarkers for carcinoma-associated fibroblasts in skin disorders including basal cell carcinoma and systemic sclerosis.[35,36]

Secreted frizzled related protein 2 (*SFRP2*) is upregulated and expression correlates with SCO severity in human fibroblasts isolated from AHO and POH participant skin biopsies

Among these differentially expressed genes, we became most interested in further examining the role of *SFRP2* in SCO pathogenesis given that it was the most upregulated gene with a known relationship to osteogenesis at the time of microarray investigation.[37] Additionally, we had identified a direct correlation between *SFRP2* mRNA expression and SCO severity by Northern blot analysis of RNA isolated from skin biopsies from 7 participants in our investigations who had either AHO or POH and 2 who were unaffected family members (described in methods) (Figure 4D). In particular, we found the highest level of *SFRP2* mRNA expression in the POH participant, intermediate expression in the AHO participant with severe ossifications, and lower levels of expression in the remaining participants with minimal, moderate, or no ossifications.

Secreted frizzled related protein 2 (*Sfrp2*) expression in *Gnas E1+/−* mouse fibroblasts correlates with expression in humans with AHO and POH

To further explore the functional role of *SFRP2* in the development of SCOs, we first assessed whether the transcriptional differences observed in human samples were similar to those within skin samples harvested from 52 wk *Gnas E1+/−* mice (Figure 4E, Figure S6). *Gnas E1+/−* mice displayed a significant upregulation of *Sfrp2* mRNA expression in dorsal skin samples containing SCOs when compared to both *WT* skin samples and *Gnas E1+/−* samples harvested from unaffected skin regions (Figure 4E). We also confirmed that the upregulation of *ARHGAP28, ALDH1A3, GPR133, ACVR2A,* and *ROR2* observed in human SCO samples was similarly observed in *Gnas E1+/−* SCO (Figure S6), demonstrating further correlation of our mouse model with the human disorder.

Based on this direct correlation of *SFRP2* expression and SCO severity in both the human and mouse samples, we assessed the spatial localization of Sfrp2 protein within the dorsal skin of 24 wk *WT* and *Gnas E1+/−* mice by immunofluorescence (Figure 4F-I). Within *WT* and unaffected *Gnas E1+/−* skin regions, Sfrp2 expression was identified within the epithelial-derived outer and inner root sheath and germinal matrix of the HF (Figure 4F-I), which is a consistent expression pattern with previous reports.[38] However, using 24 wk *Gnas E1+/−;Osx-mCherry* mice, SCO-containing skin samples revealed a markedly different Sfrp2 expression pattern (Figure 4J and K), with expansion of Sfrp2+ cellular populations along the basal epithelial surface and dispersed in the adjacent dermis from SCO sites near HFs. Of note, this enhanced Sfrp2 expression pattern that we observed in the skin has been similarly observed in both human tissue samples and animal models of systemic sclerosis,[35,36] in addition to animal models of tissue fibrosis.[39] Importantly, we detected limited co-expression of Sfrp2 within αSMA+, Osterix+ double-positive cells on the SCO

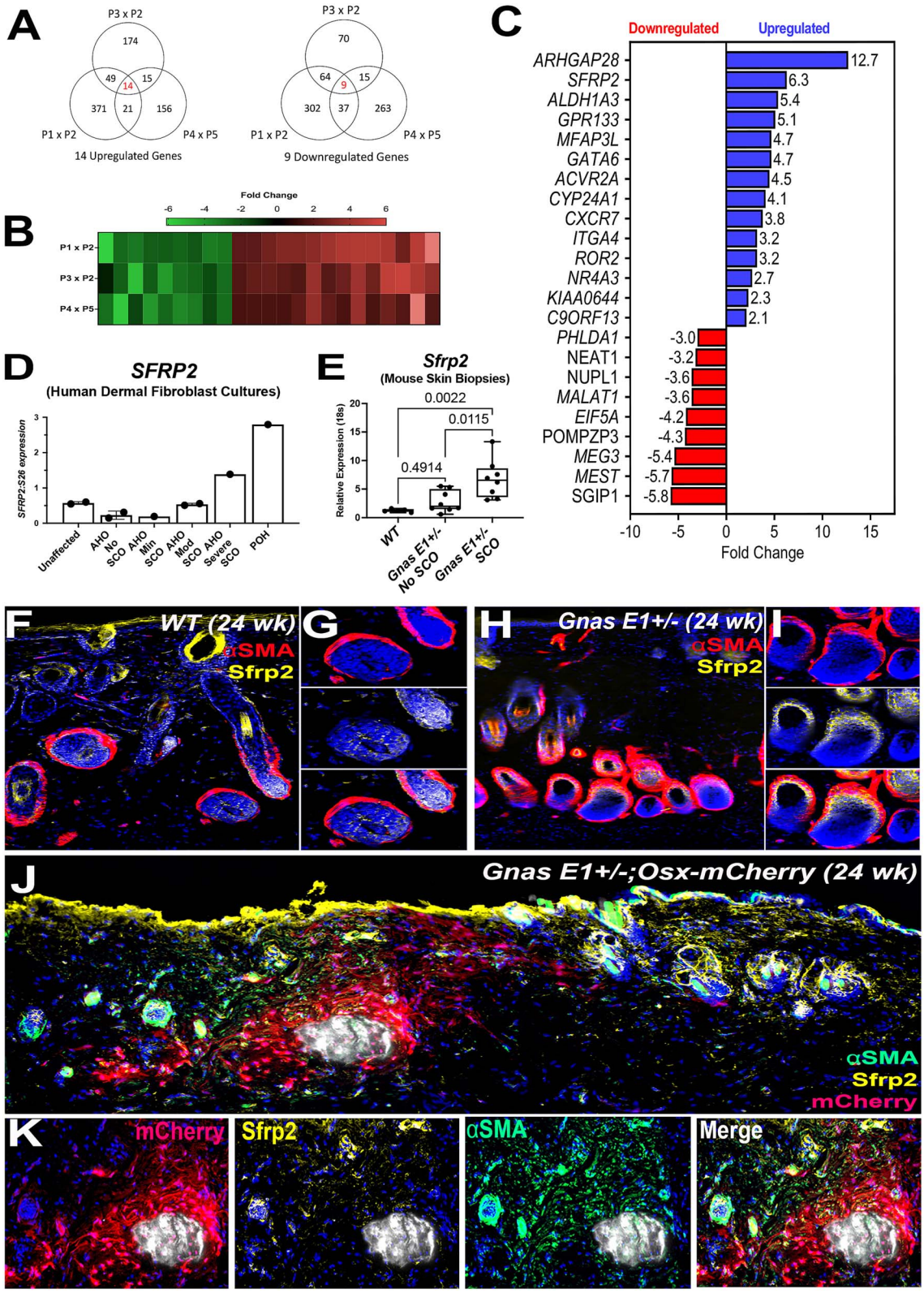

Figure 4. Microarray analyses of AHO/POH human dermal fibroblasts demonstrate upregulation of *SFRP2* expression with transcriptional profiles in SCO-containing regions consistent with *Gnas E1+/–* murine profiles. (A) Venn diagram of differentially regulated genes between 3 microarray analyses from RNA isolated from AHO and POH human dermal fibroblast cultures. (B) Representative heatmap. (C) Listing of commonly differentially regulated genes among the 3 microarray comparisons. (D) Quantification of northern blot data of *SFRP2* expression relative to *S26* from AHO and POH human dermal fibroblasts. (E) RT-PCR of *Sfrp2* expression for 52 wk WT and *Gnas* E1+/– mouse skin samples. (F-I) Low and high magnification of dorsal skin of 24 wk (F,G) WT and (H,I) *Gnas E1+/–* mice stained with Sfrp2 (yellow) and αSMA (red). (J,K) Low and high magnification images of dorsal skin section of 24 wk *Gnas E1+/–;Osx-mCherry* mouse SCO skin stained with Sfrp2 (yellow) and αSMA (green). Abbreviations: AHO, Albright hereditary osteodystrophy; POH, progressive osseous heteroplasia; SCO, subcutaneous ossification; *SFRP2, secreted frizzled related protein 2*.

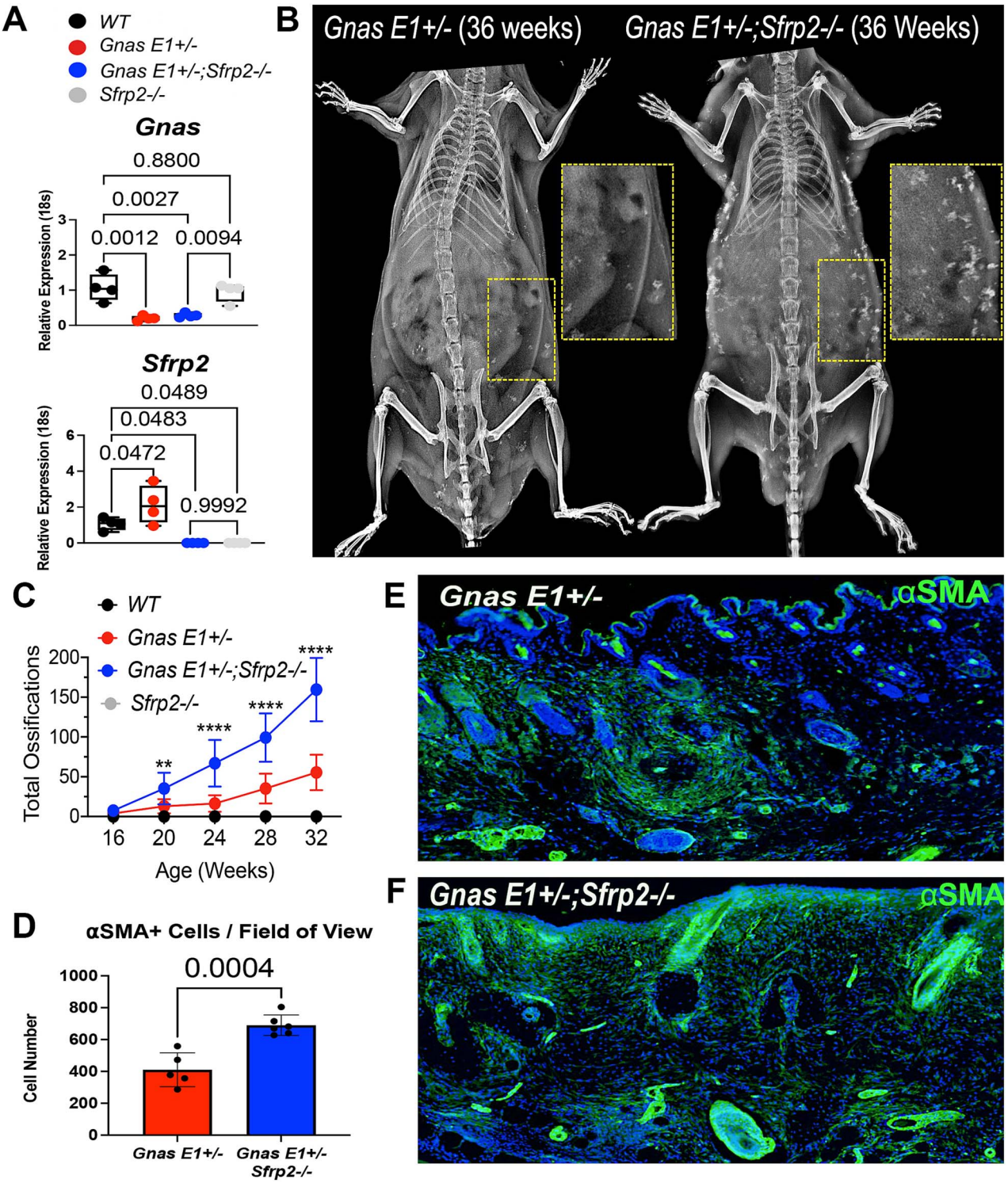

Figure 5. Global deletion of *Sfrp2* in *Gnas E1+/–* mice leads to earlier onset and accelerated formation of SCOs. (A) RT-PCR of *Gnas* and *Sfrp2* mRNA expression within 24 wk *WT, Gnas E1+/–, Gnas E1+/–;Sfrp2–/–* and *Sfrp2–/–* skin samples. (B) Representative X-ray of 36 wk male *Gnas E1+/–* and *Gnas E1+/–;Sfrp2–/–* mice demonstrating SCO formation. (C) Quantification of SCOs within male *Gnas E1+/–* and *Gnas E1+/–;Sfrp2–/–* mice following serial X-ray imaging. (**$p<.01$, and ****$p<.0001$). (D) Bar graph and (E,F) histology images of dorsal skin of SCO skin regions of 24 wk old male (E) *Gnas E1+/–* and (F) *Gnas E1+/–;Sfrp2–/–* mice stained with αSMA (green). Abbreviations: αSMA, alpha-smooth muscle actin; SCO, subcutaneous ossification.

bone-lining surface (Figure 4J and K). Given that SCO-containing skin regions exhibit a broader expression of Sfrp2 near HFs and that our previous studies had found SCOs consistently developing adjacent to or surrounding HFs, we further examined the contribution of HF cellular populations to SCO formation and how Sfrp2 may influence the differentiation capacity of heterogenous accessory cell types within this microenvironment.

Global deletion of *Sfrp2* in *Gnas E1+/−* mice leads to earlier onset and accelerated formation of SCOs

Finally, we investigated the functional role of SFRP2 in SCO development based on our initial findings showing increased *SFRP2* expression in fibroblasts isolated from AHO patients, which we also observed in our mouse model. We first carried out cell culture studies using mouse dermal explants (Figure S7). Although we observed increased collagen matrix deposition in *Gnas E1+/−* explants compared to *WT*, addition of recombinant SFRP2 to these cultures had no effect on matrix deposition, mineralization, osteogenic differentiation, or *Alpl, Sp7 (Osterix)*, and *Ibsp* gene expression.

We next investigated the role of Sfrp2 in SCO formation in vivo by crossing *Sfrp2−/−* mice[40] with *Gnas E1+/−* mice. *Sfrp2* deletion was confirmed in *Gnas E1+/−;Sfrp2−/−* and *Sfrp2−/−* mice by RT-PCR (Figure 5A). We examined the rate of SCO formation in both male (Figure 5B and C) and female (Figure S7D) *Gnas E1+/−* and *Gnas E1+/−;Sfrp2−/−* mice by serial radiographic imaging every 4 wk starting at 16 wk of age. As expected, we did not observe SCO formation in male or female *WT* or *Sfrp2−/−* mice (data not shown); however, we could readily detect SCOs in both *Gnas E1+/−* and *Gnas E1+/−;Sfrp2−/−* mice (Figure 5B and C). As described previously, *Gnas E1+/−* female mice developed fewer SCOs compared to male mice[12] and we did not observe any significant differences in SCO formation between female *Gnas E1+/−* and *Gnas E1+/−;Sfrp2−/−* mice (Figure S7D). However, male *Gnas E1+/−;Sfrp2−/−* mice developed SCOs significantly earlier than *Gnas E1+/−* mice and also developed a greater number of total SCOs by 20 wk of age that continued to increase at each subsequent timepoint (Figure 5C).

Global deletion of *Sfrp2* in *Gnas E1+/−* mice expands αSMA+ populations in dorsal skin and basal epithelial surface

In alignment with their accelerated rate of SCO formation, we observed that male *Gnas E1+/−;Sfrp2−/−* mice displayed an expansion in the number of αSMA+ populations throughout the dorsal skin and along the basal epithelial surface when compared to *Gnas E1+/−* mice (Figure 5D-F). The expanded αSMA+ populations in *Gnas E1+/−;Sfrp2−/−* were observed within the basal epithelial surface as well as within epithelial-derived HF populations when compared to *Gnas E1+/−* αSMA+ populations that were limited to the dermis (Figure 5D-F). Collectively, these data demonstrate that loss of Sfrp2 exacerbates the development of SCO formation in *Gnas E1+/−* mice and suggests that *SFRP2* upregulation in AHO may be a compensatory mechanism that limits SCO formation.

Discussion

Our data are the first to provide direct evidence that SCO formation in *Gnas E1+/−* mice is initiated by the inappropriate expansion and differentiation of HF-resident αSMA-expressing dermal sheath cells into osteoblasts. These findings correlate with clinical observations in patients with AHO in whom SCOs develop within the dermis and subcutaneous tissue and do not penetrate underlying fascial planes.

We utilized an *Osterix-mCherry* transgenic reporter system[16] to characterize the presence of dermal-resident cell types that may lead to SCO formation. Osterix has been recognized as an indispensable transcription factor necessary for the commitment of mesenchymal progenitors to the osteogenic lineage and to osteoblast differentiation. Our investigations led to the identification of Osterix+ cell types within the HF of both *WT* and *Gnas E1+/−* mice. These data align with prior studies demonstrating postnatal extraskeletal Osterix expression in tissues such as olfactory glomerular cells,[41] intestinal crypt stem cells,[42] and the renal proximal convoluted tubules.[16] Given that the HF contains multiple epithelial- and mesenchymal-derived progenitors, we performed immunofluorescence co-localization studies and identified that these Osterix+ cells specifically corresponded to mesenchymal-derived dermal sheath cells in the HF based on the co-expression studies with αSMA.

The dermal sheath has recently been recognized as a substantial source of mesenchymal progenitors within the HF that exhibit high plasticity and self-renewal capacity throughout adulthood (for review, see[43]). In vivo fate-mapping studies of dermal sheath cells using a tamoxifen-inducible *αSMACreER^{T2};YFP* mouse model have demonstrated that there is a subset of dermal sheath cells that can regenerate out to 24 mo post tamoxifen injection and differentiate and repopulate into multiple cell types within the regenerating HF.[27] In addition, studies have shown that human- and rat-derived dermal sheath cells can differentiate into adipocytes, osteoblasts, and chondrocytes in vitro.[44] These data, in conjunction with our genetic fate-mapping studies demonstrating that *Gnas E1+/−* dermal sheath cells differentiate into osteoblasts and osteocytes, further emphasize their plasticity. Future transplantation studies assessing the osteogenic capacity of purified dermal sheath cells using methods such as subcutaneous implantation or calvarial defect models are warranted.

Our histologic evaluation of the dermis in 40 wk old *Gnas E1+/−;Osx-mCherry* and *Gnas E1+/−;αSMACre^{ERT2};Ai9$^{fl/fl}$* mice within SCO-containing regions identified focally diffuse Osterix+ or Ai9+ populations dispersed throughout the surrounding epidermis and dermis. These observations directly correlate with prior fate-mapping studies that have shown that in postnatal *Gnas* homozygous deletion models, initial heterotopic bone formation is driven by the osteogenic differentiation of local mesenchymal progenitors; however, the progressive expansion of these lesions over time is driven by the recruitment of surrounding cell types to the lesion site for subsequent osteogenic differentiation.[45,46] Collectively, our data build upon the preexisting literature and further suggest that heterotopic bone formation requires a delicate combination of both mutated cells and an altered signaling milieu within the surrounding tissue environment.

In conjunction with assessing the cellular populations that contribute to SCO formation, we also identified significant variations in Shh, TGF-β, BMP, and Wnt signaling activity within SCO-containing skin regions of *Gnas E1+/−* mice by RT-PCR array and immunofluorescence. These data are of particular interest given that these pathways have been shown to contribute to the pathogenesis of trauma-induced HOs[1] but to date have not been fully implicated in the context of ossification formation in AHO or POH. Consequently, further studies are warranted to further understand the role of

the $G\alpha_s$-PKA-cAMP signaling cascade in mediating epithelial-mesenchymal interactions within the HF microenvironment. Additionally, despite these encouraging data, it is also important to acknowledge that these findings are representative of the global transcriptional changes within the skin at 52 wk of age with the presence of established SCOs contained within the dermis. To this point, it is likely that there are additional and alternative contributing pathways throughout the various stages of SCO development that are restricted to specific timeframes, tissue microenvironments, and/or individual cell populations that may not be most representative within this current data set. Consequently, these data pose an interesting set of additional questions into the spatiotemporal activation of varying cell types involved in the pathogenesis of heterotopic bone formation that warrants further exploration though the use of techniques such as single cell RNA sequencing and spatial transcriptomics.

Finally, we had carried out microarray analysis of RNA from dermal fibroblast cultures derived from skin biopsies from patients with AHO and POH presenting with varying degrees of SCOs. By comparing gene expression profiles from these patients, we had identified a direct correlation between *SFRP2* mRNA expression and SCO severity. Although SFRP2 was initially characterized as a secreted protein that competitively binds and inhibits ligands essential for canonical Wnt signaling,[31,33,34] more recent studies have identified this protein to function as both an agonist and antagonist of Wnt signaling dependent upon its context and has been shown to directly influence epithelial proliferation, epithelial to mesenchymal transition, and skin fibrosis.[36,38,39,47,48] We also analyzed *Sfrp2* expression in the skin of *Gnas E1+/−* mice and similarly found strong expression within the HF and its surrounding dermis and basal epithelium. Our findings could be consistent either with *SFRP2* playing a causal role in the initiation of SCO development or with *SFRP2* upregulation being a response to mitigate further SCO formation. In order to distinguish these 2 possibilities, we investigated the development of SCOs in *Gnas E1+/−;Sfrp2−/−* mice. We found that loss of *Sfrp2* accelerated the development of SCOs resulting from heterozygous loss of *Gnas* in terms of both age of onset and total number in male mice. In light of our in vivo observations, we hypothesize at this time that *Sfrp2*, with its expression within ossification-containing regions, may potentially function as a paracrine-secreted factor from the surrounding epithelium to inhibit osteogenic differentiation of αSMA+ dermal sheath cells. The finding that *Gnas E1+/−* male mice develop more SCOs compared to females correlates with our prior studies,[12] including those in humans with AHO,[13] and requires further investigation. Our results imply that the upregulation of *SFRP2* observed in both humans and mice likely represents a compensatory mechanism that limits further SCO development and/or progression. This hypothesis is in alignment with previous reports of pathologic states including multiple myeloma and amelobastoma demonstrating that *Sfrp2* expression negatively regulates osteoblast differentiation and function.[37,49] Our findings raise the possibility that administration of SFRP2 or a functional agonist may be a potential therapeutic strategy for the prevention and treatment of HOs.

Acknowledgments

We sincerely thank the patients and their families who made this work possible. We also thank the Johns Hopkins University School of Medicine Institute of Clinical and Translational Research and the Johns Hopkins Microarray Core Facility, as well as Evan Jellison and the UConn Health Flow Cytometry Core Facility for their assistance in a portion of these studies.

Author contributions

P.Mc., P.Ma., S.R., I.K., D.R., and E.L.G.-L. contributed to study design. P.Mc., S.R., S. E., Q.Y., and E.L.G.-L. conducted the experimental investigations, collected data, and performed data analysis. P.Mc. and E.L.G.-L. wrote the initial manuscript. P.Mc., P.Ma., S.R., S.E., I.K., and E.L.G.-L. critically revised the manuscript. All authors reviewed the draft of the manuscript.

Patrick McMullan (Conceptualization, Data curation, Formal analysis, Investigation, Methodology, Validation, Visualization, Writing—original draft preparation, Writing—review & editing), Peter Maye (Methodology, Project administration, Resources, Supervision, Validation, Writing—review & editing), Sierra Root (Methodology, Data curation, Formal analysis, Investigation, Validation, Visualization, Writing—review & editing), Qingfen Yang (Data curation, Investigation, Methodology, Validation, Writing—review), Sarah Edie (Data curation, Investigation, Validation, Writing—review & editing), David W. Rowe (Methodology, Resources, Supervision, Validation, Writing—review), Ivo Kalajzic (Methodology, Resources, Supervision, Validation, Writing—review & editing), and Emily L. Germain-Lee (Conceptualization, Data curation, Formal analysis, Funding acquisition, Investigation, Methodology, Project administration, Resources, Supervision, Validation, Visualization, Writing—original draft preparation, Writing—review &editing).

Supplementary material

Supplementary material is available at *JBMR Plus* online.

Funding

This work was supported in part by US Food and Drug Administration Office of Orphan Products Development Grants R01 FD-R-002568 and R01 FD-R-003409 (to E.L.G.-L.), Thrasher Research Foundation Grant 02818-8 (to E.L.G.-L.), National Institutes of Health Grant R21 HD078864 (to E.L.G.-L.), R01 AR081659 (to E.L.G.-L.), and M01 RR00052 (to the Johns Hopkins University School of Medicine Institute of Clinical and Translational Research). P.M. was supported by a training grant from the NIH: NIDCR 640T90DE021989-09.

Conflicts of interest

None declared.

Data availability

The data underlying this article will be shared upon request to the corresponding author.

References

1. Meyers C, Lisiecki J, Miller S, et al. Heterotopic ossification: a comprehensive review. *JBMR Plus*. 2019;3(4):e10172. https://doi.org/10.1002/jbm4.10172
2. Cappato S, Gamberale R, Bocciardi R, Brunelli S. Genetic and acquired heterotopic ossification: a translational tale of mice and men. *Biomedicines*. 2020;8(12):1–20.
3. Shore EM, Xu M, Feldman GJ, Fenstermacher DA, Brown MA, Kaplan FS. A recurrent mutation in the BMP type I receptor ACVR1 causes inherited and sporadic fibrodysplasia ossificans progressiva. *Nat Genet*. 2006;38(5):525–527. https://doi.org/10.1038/ng1783

4. Plagge A, Kelsey G, Germain-Lee EL. Physiological functions of the imprinted Gnas locus and its protein variants Gαs and XLαs in human and mouse. *J Endocrinol*. 2008;196(2):193–214.
5. Bastepe M. GNAS mutations and heterotopic ossification. *Bone*. 2018;109:80–85. https://doi.org/10.1016/j.bone.2017.09.002
6. McMullan P, Germain-Lee EL. Aberrant bone regulation in Albright hereditary osteodystrophy due to Gnas inactivation: mechanisms and translational implications. *Curr Osteoporos Rep*. 2022;20(1):78–89.
7. Germain-Lee EL, Levine MA. Pseudohypoparathyroidism. In: Bilezlkian J, ed. *Prim. Metab. Bone Dis. Disord. Miner. Metab*. 10th ed. Wolters Kluwer; 2025:615–628.
8. Kaplan FS, Shore EM. Progressive osseous heteroplasia. *J Bone Miner Res*. 2000;15(11):2084–2094.
9. Pignolo RJ, Ramaswamy G, Fong JT, Shore EM, Kaplan FS. Progressive osseous heteroplasia: diagnosis, treatment, and prognosis. *Appl Clin Genet*. 2015;8:37–48. https://doi.org/10.2147/TACG.S51064
10. Eddy MC, Jan de Beur SM, Yandow SM, et al. Deficiency of the α-subunit of the stimulatory G protein and severe extraskeletal ossification. *J Bone Miner Res*. 2000;15(11):2074–2083.
11. Lin MH, Numbenjapon N, Germain-Lee EL, Pitukcheewanont P. Progressive osseous heteroplasia, as an isolated entity or overlapping with Albright hereditary osteodystrophy. *J Pediatr Endocrinol Metab*. 2015;28(7–8):911–918.
12. Huso DL, Edie S, Levine MA, et al. Heterotopic ossifications in a mouse model of Albright hereditary osteodystrophy. *PLoS One*. 2011;6(6):e21755. https://doi.org/10.1371/journal.pone.0021755
13. Salemi P, Olson JMS, Dickson LE, Germain-Lee EL. Ossifications in Albright hereditary osteodystrophy: role of genotype, inheritance, sex, age, hormonal status, and BMI. *J Clin Endocrinol Metab*. 2018;103(1):158–168. https://doi.org/10.1210/jc.2017-00860
14. Germain-Lee EL, Schwindinger W, Crane JL, et al. A mouse model of Albright hereditary osteodystrophy generated by targeted disruption of exon 1 of the Gnas gene. *Endocrinology*. 2005;146(11):4697–4709. https://doi.org/10.1210/en.2005-0681
15. Rendl M, Lewis L, Fuchs E. Molecular dissection of mesenchymal–epithelial interactions in the hair follicleHogan B, editor. *PLoS Biol*. 2005;3(11):e331.
16. Strecker S, Fu Y, Liu Y, Maye P. Generation and characterization of Osterix-Cherry reporter mice. *Genesis*. 2013;51(4):246–258.
17. Grcevic D, Pejda S, Matthews BG, et al. In vivo fate mapping identifies mesenchymal progenitor cells. *Stem Cells*. 2012;30(2):187–196.
18. Dyment NA, Jiang X, Chen L, et al. High-throughput, multi-image cryohistology of mineralized tissues. *J Vis Exp*. 2016;115:54468
19. McMullan P, Maye P, Yang Q, Rowe DW, Germain-Lee EL. Parental origin of Gsα inactivation differentially affects bone remodeling in a mouse model of Albright hereditary osteodystrophy. *JBMR Plus*. 2021;6(1):e10570.
20. Walmsley GG, Maan ZN, Hu MS, et al. Murine dermal fibroblast isolation by FACS. *J Vis Exp*. 2016;107:53430.
21. Seluanov A, Vaidya A, Gorbunova V. Establishing primary adult fibroblast cultures from rodents. *J Vis Exp*. 2010;44:2033.
22. López-De León A, Rojkind M. A simple micromethod for collagen and total protein determination in formalin-fixed paraffin-embedded sections. *J Histochem Cytochem*. 1985;33(8):737–743.
23. Germain-Lee EL, Groman J, Crane JL, Jan de Beur SM, Levine MA. Growth hormone deficiency in pseudohypoparathyroidism type 1a: another manifestation of multihormone resistance. *J Clin Endocrinol Metab*. 2003;88(9):4059–4069. https://doi.org/10.1210/jc.2003-030028
24. Germain-Lee EL. Short stature, obesity, and growth hormone deficiency in pseudohypoparathyroidism type 1a. *Pediatr Endocrinol Rev*. 2006;3(2):318–327.
25. Hsu SC, Groman JD, Merlo CA, et al. Patients with mutations in Gsalpha have reduced activation of a downstream target in epithelial tissues due to haploinsufficiency. *J Clin Endocrinol Metab*. 2007;92(10):3941–3948.
26. Germain-Lee EL, Obie C, Valle D. NVL: a new member of the AAA family of ATPases localized to the nucleus. *Genomics*. 1997;44(1):22–34.
27. Rahmani W, Abbasi S, Hagner A, et al. Hair follicle dermal stem cells regenerate the dermal sheath, repopulate the dermal papilla, and modulate hair type. *Dev Cell*. 2014;31(5):543–558. https://doi.org/10.1016/j.devcel.2014.10.022
28. Kalajzic Z, Li H, Wang LP, et al. Use of an alpha-smooth muscle actin GFP reporter to identify an osteoprogenitor population. *Bone*. 2008;43(3):501–510.
29. Matthews BG, Torreggiani E, Roeder E, Matic I, Grcevic D, Kalajzic I. Osteogenic potential of alpha smooth muscle actin expressing muscle resident progenitor cells. *Bone*. 2015;84:69–77. https://doi.org/10.1016/j.bone.2015.12.010
30. Plikus MV. New activators and inhibitors in the hair cycle clock: targeting stem cells state of competence. *J Invest Dermatol*. 2012;132(5):1321–1324. https://doi.org/10.1038/jid.2012.38
31. Rattner A, Hsieh JC, Smallwood PM, et al. A family of secreted proteins contains homology to the cysteine-rich ligand-binding domain of frizzled receptors. *Proc Natl Acad Sci USA*. 1997;94(7):2859–2863.
32. Yeung C-YC, Taylor SH, Garva R, et al. Arhgap28 is a RhoGAP that inactivates RhoA and downregulates stress fibersHotchin NA, editor. *PLoS One*. 2014;9(9):e107036.
33. He W, Zhang L, Ni A, et al. Exogenously administered secreted frizzled related protein 2 (Sfrp2) reduces fibrosis and improves cardiac function in a rat model of myocardial infarction. *Proc Natl Acad Sci USA*. 2010;107(49):21110–21115.
34. Wei W-Y, Zhao Q, Zhang W-Z, et al. Secreted frizzled-related protein 2 prevents pressure-overload-induced cardiac hypertrophy by targeting the Wnt/ β-catenin pathway. *Mol Cell Biochem*. 2020;472(1-2):241–251. https://doi.org/10.1007/s11010-020-03802-x
35. Micke P, Kappert K, Ohshima M, et al. In situ identification of genes regulated specifically in fibroblasts of human basal cell carcinoma. *J Invest Dermatol*. 2007;127(6):1516–1523. https://doi.org/10.1038/sj.jid.5700714
36. Tabib T, Huang M, Morse N, et al. Myofibroblast transcriptome indicates SFRP2hi fibroblast progenitors in systemic sclerosis skin. *Nat Commun*. 2021;12(1):1–13.
37. Oshima T, Abe M, Asano J, et al. Myeloma cells suppress bone formation by secreting a soluble Wnt inhibitor, sFRP-2. *Blood*. 2005;106(9):3160–3165.
38. Kim B-K, Yoon SK. Expression of sfrp2 is increased in catagen of hair follicles and inhibits keratinocyte proliferation. *Ann Dermatol*. 2014;26(1):79–87. https://doi.org/10.5021/ad.2014.26.1.79
39. Dolivo DM, Rodrigues AE, Sun LS, Mustoe TA, Hong SJ, Galiano RD. Skin fibrosis is accompanied by increased expression of secreted frizzled-related protein-2. *Wound Repair Regen*. 2024;32(5):720–724. https://doi.org/10.1111/wrr.13211
40. Morello R, Bertin TK, Schlaubitz S, et al. Brachy-syndactyly caused by loss of Sfrp2 function. *J Cell Physiol*. 2008;217(1):127–137.
41. Chen J, Shi Y, Regan J, Karuppaiah K, Ornitz DM, Long F. Osx-Cre targets multiple cell types besides osteoblast lineage in postnatal mice. *PLoS One*. 2014;9(1):e85161.
42. Wang L, Moore DC, Huang J, et al. SHP2 regulates the development of intestinal epithelium by modifying OSTERIX $^{+}$ crypt stem cell self-renewal and proliferation. *FASEB J*. 2021;35(1):e21106.
43. Martino PA, Heitman N, Rendl M. The dermal sheath: an emerging component of the hair follicle stem cell niche. *Exp Dermatol*. 2020;30(4):512–521.
44. Jahoda CAB, Whitehouse CJ, Reynolds AJ, Hole N. Hair follicle dermal cells differentiate into adipogenic and osteogenic lineages.

Exp Dermatol. 2003;12(6):849–859. https://doi.org/10.1111/j.0906-6705.2003.00161.x
45. Brewer N, Fong JT, Zhang D, Ramaswamy G, Shore EM. Gnas inactivation alters subcutaneous tissues in progression to heterotopic ossification. *Front Genet*. 2021;**12**:633206.
46. Cong Q, Liu Y, Zhou T, et al. A self-amplifying loop of YAP and SHH drives formation and expansion of heterotopic ossification. *Sci Transl Med*. 2021;13(599):2233.
47. Zeng X, Zhang Y, Xu H, Zhang T, Xue Y, An R. Secreted frizzled related protein 2 modulates epithelial–mesenchymal transition and stemness via Wnt/β-catenin signaling in choriocarcinoma. *Cell Physiol Biochem*. 2018;50(5):1815–1831. https://doi.org/10.1159/000494862
48. Tabib T, Morse C, Wang T, Chen W, Lafyatis R. SFRP2/DPP4 and FMO1/LSP1 define major fibroblast populations in human skin. *J Invest Dermatol*. 2018;138(4):802–810. https://doi.org/10.1016/j.jid.2017.09.045
49. Sathi GA, Inoue M, Harada H, et al. Secreted frizzled related protein (sFRP)-2 inhibits bone formation and promotes cell proliferation in ameloblastoma. *Oral Oncol*. 2009;45(10):856–860.

JBMR Plus, 2025, 9, ziaf038
https://doi.org/10.1093/jbmrpl/ziaf038
Research Article